Hybrid Analysis of Three-Dimensional MMIC Elements by the Method of Lines

Larissa Vietzorreck, *Member, IEEE,* and Reinhold Pregla, *Senior Member, IEEE*

***Abstract*—A new eigenmode algorithm, based on the method of lines, is presented for full-wave analysis of real three-dimensional (3-D) MMIC elements. Finite conductor thickness, finite substrate, dielectric or ohmic losses are rigorously modeled. The analytical calculation in the direction of propagation enables the analysis of structures with very short or long interconnections between the single discontinuities. To demonstrate the generality of the proposed algorithm several completely different structures were analyzed. Examinations of the convergence were performed. Scattering parameters of filters and planar transmission line interconnects like air bridges, via holes and bead transitions were investigated. The calculated results agree very well with computed and measured results published in literature.**

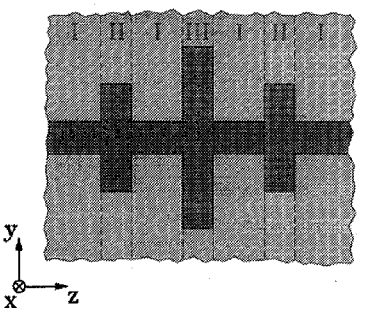

Fig. 1. Top view of an example.

I. Introduction

In the design of planar integrated circuits discontinuities of metallization and substrate occur at several parts of the devices, causing reflections and disturbing the propagation. In designing filter elements these effects are used to achieve a certain behavior of the circuit, others are caused by the construction itself and should be avoided as much as possible, like in transitions of different types of transmission lines. In packed structures the transmission lines in different layers can be connected by via holes, a connection to a chip can be done by air bridges or bondwires and, if single components of the circuits are encapsulated, special forms of transitions through a wall are needed. All these transitions are three-dimensional (3-D), even though the connected circuits are planar. The intended electrical performance of the microwave device may be severely deteriorated, if the design of the described elements is made improperly. Hence an accurate analysis of a wide class of complex 3-D elements encountered in practice is necessary.

Some of these interconnecting structures or filter elements have been investigated by various methods, e.g., FD [1], [2], FEM [3], FDTD [4], TLM [5], or SDA [6]. In these methods problems may occur in the modeling of a finite substrate, a finite conductor thickness or in the analysis of very short or long interconnections. Additionally, in some methods artificial boundaries have to be provided at the input and output.

It has been shown in numerous papers, that the method of lines (MoL) is highly suitable for analysis of planar transmission lines [7]. In the design of microwave circuits, however, the MoL has been applied mostly to planar structures with few discontinuities, using a two-dimensional (2-D) discretization perpendicular to the propagation direction [8], [9]. As a consequence of this form of discretization the size of the calculation window increases very much for longitudinally inhomogeneous structures and special boundary conditions for the boundaries in propagation direction have to be established.

Another approach is the division of a structure in cascaded subsections with respect to the propagation direction. This procedure has been successfully applied to dielectric waveguide structures in integrated optics [10] and to homogeneously filled waveguides [11]. In the analysis of the optical structures, however, not all reflections were considered.

Recently, single planar microstrip discontinuities have been studied by the MoL using discretization lines in propagation direction [12]. In this paper this new approach is substantially extended for the analysis of cascaded discontinuities with 3-D metallizations. The difficulties relevant to the above mentioned methods are eliminated. Finite as well as zero conductor thickness, finite substrate, dielectric or ohmic losses are rigorously modeled by a 2-D discretization of the cross section. The analytical calculation in the direction of propagation enables the analysis of structures with very short or long interconnections between the single discontinuities. In the analysis all eigenmodes are considered. High accuracy of the calculation is achieved by matching the field components instead of the modes.

II. Theory

In contrast to the conventional MoL the examined structure is not divided into layers but into a series of sections with a longitudinally homogeneous distribution of dielectric media and metallization (see Fig. 1).

The finite conductor thickness and the finite and/or inhomogeneous substrate are modeled by a 2-D distribution of the permittivity and the metallization within the cross section (see

Manuscript received April 1, 1996. This work was supported by a Grant of the Deutsche Forschungsgemeinschaft.

The authors are with the Department of Electrical Engineering, FernUniversität, Hagen, Germany.

Publisher Item Identifier S 0018-9480(96)08572-9.

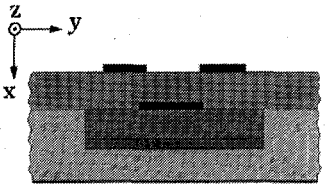

Fig. 2. Cross section of an example.

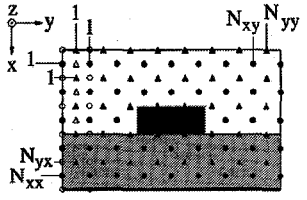

- $\bullet$ ϕ_z, $\mathbf{E}_x$, $\mathbf{H}_y$, $\varepsilon_\bullet$
- $\blacktriangle$ ϕ_y, $\mathbf{E}_y$, $\mathbf{H}_x$, $\varepsilon_\blacktriangle$
- $\circ$ $\dfrac{\partial \phi_x}{\partial x}$, $\dfrac{\partial \phi_y}{\partial y}$, $\mathbf{E}_z$, $\varepsilon_\circ$
- $\triangle$ $\dfrac{\partial \phi_x}{\partial y}$, $\dfrac{\partial \phi_y}{\partial x}$, $\mathbf{H}_z$, $\varepsilon_\triangle$

Fig. 3. Discretization scheme.

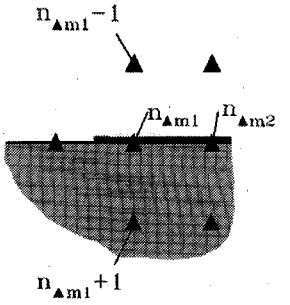

Fig. 4. Discretization points on the metallization.

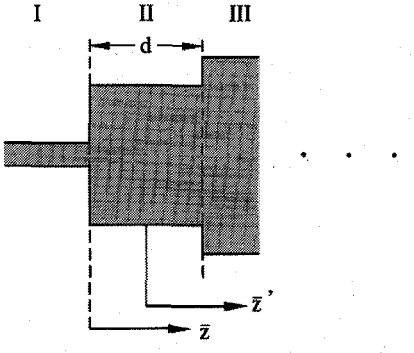

Fig. 5. Position of the coordinate origin.

Fig. 2). Dielectric and ohmic losses can be considered using complex permittivities.

A. Calculation of the Eigenvalues

In each longitudinally homogeneous section the electromagnetic field is derived from a vector potential $\mathbf{\Pi}$. It is important that the potential has the same vector components as the gradient of the permittivity of the material ε_r.

$$\mathbf{\Pi} = \phi_x \cdot \mathbf{e}_x + \phi_y \cdot \mathbf{e}_y. \tag{1}$$

Only this general solution leads to a consistent system of coupled differential equations of the Sturm–Liouville type for the potential components ϕ_x and ϕ_y. The coordinates are normalized according to $\overline{x} = k_0 x$, $\overline{y} = k_0 y$, $\overline{z} = k_0 z$.

$$\frac{\partial^2}{\partial \overline{z}^2}\phi_x + \frac{\partial^2}{\partial \overline{y}^2}\phi_x + \epsilon_r \frac{\partial}{\partial \overline{x}}\left[\epsilon_r^{-1}\left(\frac{\partial \phi_x}{\partial \overline{x}} + \frac{\partial \phi_y}{\partial \overline{y}}\right)\right] + \epsilon_r \phi_x - \frac{\partial}{\partial \overline{y}}\left(\frac{\partial \phi_y}{\partial \overline{x}}\right) = 0 \tag{2}$$

$$\frac{\partial^2}{\partial \overline{z}^2}\phi_y + \frac{\partial^2}{\partial \overline{x}^2}\phi_y + \epsilon_r \frac{\partial}{\partial \overline{y}}\left[\epsilon_r^{-1}\left(\frac{\partial \phi_y}{\partial \overline{y}} + \frac{\partial \phi_x}{\partial \overline{x}}\right)\right] + \epsilon_r \phi_y - \frac{\partial}{\partial \overline{x}}\left(\frac{\partial \phi_x}{\partial \overline{y}}\right) = 0. \tag{3}$$

The cross section of each section is now subjected to a 2-D discretization, the solution in propagation direction being analytical. We use four different line systems for the potentials ϕ_x and ϕ_y and their derivatives which are shifted toward each other. The 2-D difference operators constructed by Kronecker products from the one-dimensional ones are described in detail in [10]. In the further analysis they are denoted by a hat ($\hat{}$).

In case of a perfectly conducting metallization the components have to fulfill the different boundary conditions for a metallic wall. These boundary conditions can easily be incorporated into the difference operators. An example for the modification of the difference operator is given by the derivative in x-direction of the component ϕ_y, fulfilling the Dirichlet boundary condition $\phi_y = 0$ at the metallization

$$\boldsymbol{D}_{yx} = \begin{bmatrix} \cdots & \phi_{ym-1} & \phi_{ym} & \phi_{ym+1} & \cdots \end{bmatrix}$$
$$\begin{bmatrix} \ddots & \ddots & & & & \\ & -1 & 1 & & & \\ & & -1 & 1 & & \\ & & & -1 & 1 & \\ & & & & -1 & 1 \\ & & & & & \ddots \end{bmatrix}^{N_{yx}}$$
$$\begin{bmatrix} \cdots & \phi_{ym-1} & \phi_{ym+1} & \cdots \end{bmatrix}$$

$$\rightarrow \quad \boldsymbol{D}^r_{yx} = \begin{bmatrix} \ddots & \ddots & & & \\ & -1 & 1 & & \\ & & -1 & & \\ & & & 1 & \\ & & & -1 & 1 \\ & & & & \ddots \end{bmatrix}^{N_{yx}-1} \tag{4}$$

A generalization of the reduction procedure can be established by introducing so-called structure matrices for each line system. The structure matrix $\hat{\boldsymbol{S}}$ for the line system of ϕ_x is derived from an identity matrix of the size $N_{xx} \cdot N_{xy}$, in which the columns corresponding to the position of the lines within

the metallization are deleted

$$\hat{\boldsymbol{S}} = \begin{bmatrix} \ddots & & & & \\ & 1 & & & \\ & & 0 & & \\ & & 1 & & \\ & & & \ddots & \\ & & \vdots & \vdots & \\ & & n_{m1}-1 & n_{m1}+1. & \end{bmatrix} \tag{5}$$

The reduced difference operators and matrices containing the discretized values of the permittivity are now easily derived from the undisturbed case by a multiplication with the different structure matrices.

$$\begin{array}{llll} \hat{\boldsymbol{D}}^r_{yy} = \boldsymbol{S}^t_{\circ} \cdot \hat{\boldsymbol{D}}_{yy} \cdot \boldsymbol{S}_{\blacktriangle} & & \hat{\varepsilon}^r_{\blacktriangle} = \boldsymbol{S}^t_{\blacktriangle} \cdot \hat{\varepsilon}_{\blacktriangle} \cdot \boldsymbol{S}_{\blacktriangle} \\ \hat{\boldsymbol{D}}^r_{yx} = \boldsymbol{S}^t_{\triangle} \cdot \hat{\boldsymbol{D}}_{yx} \cdot \boldsymbol{S}_{\blacktriangle} & & \hat{\varepsilon}^r_{\circ} = \boldsymbol{S}^t_{\circ} \cdot \hat{\varepsilon}_{\circ} \cdot \boldsymbol{S}_{\circ} \\ \hat{\boldsymbol{D}}^r_{xx} = \boldsymbol{S}^t_{\circ} \cdot \hat{\boldsymbol{D}}_{xx} \cdot \boldsymbol{S}_{\bullet} & & \hat{\varepsilon}^r_{\bullet} = \boldsymbol{S}^t_{\bullet} \cdot \hat{\varepsilon}_{\bullet} \cdot \boldsymbol{S}_{\bullet} \\ \hat{\boldsymbol{D}}^r_{xy} = \boldsymbol{S}^t_{\triangle} \cdot \hat{\boldsymbol{D}}_{xy} \cdot \boldsymbol{S}_{\bullet} & & \end{array} \tag{6}$$

Transforming the discretized wave equation to principal axes gives a system of uncoupled differential equations

$$\frac{\partial^2}{\partial \overline{z}^2} \hat{\overline{\mathbf{\Pi}}} - \hat{\Gamma}^2 \hat{\overline{\mathbf{\Pi}}} = \mathbf{0} \tag{7}$$

with

$$\hat{\mathbf{\Pi}} = \hat{T} \hat{\overline{\mathbf{\Pi}}} \qquad \hat{T}^{-1} \hat{\boldsymbol{Q}} \hat{T} = \hat{\Gamma}^2 \tag{8}$$

where the vector $\hat{\mathbf{\Pi}}$ contains the discretized and reduced potential components of ϕ_x and ϕ_y. A detailed description of the components of the coupling matrix $\boldsymbol{Q}$ can be found in Appendix A.

The solution for the transformed potential yields

$$\hat{\overline{\mathbf{\Pi}}}(\overline{z}) = e^{-\hat{\Gamma}\overline{z}}\mathbf{A} + e^{\hat{\Gamma}\overline{z}}\mathbf{B} \tag{9}$$

or

$$\hat{\overline{\mathbf{\Pi}}}(\overline{z}) = \cosh(\hat{\Gamma}\overline{z}')\mathbf{A} + \sinh(\hat{\Gamma}\overline{z}')\mathbf{B} \tag{10}$$

with the position of the different coordinate origins in $\overline{z}$, $\overline{z}'$ given in Fig. 5. In the outer sections the first formulation is chosen. $\mathbf{A}$ and $\mathbf{B}$ denote the amplitudes of the forward and backward going waves and $\hat{\Gamma}$ is a diagonal matrix, containing the normalized propagation constants in z direction, including evanescent and complex modes. For the inner sections the second formulation is numerically favorable.

B. Matching Procedure

Matching the tangential field components at one interface establishes a relation between the amplitudes $\mathbf{A}$ and $\mathbf{B}$ in both sections. The resulting scattering matrix for one discontinuity can be carried out as described in [12]. For structures with several discontinuities, when (10) is used to describe the transformed potential in the inner sections, we use the following formulation for the fields in the matching plane

$$\begin{aligned} \mathbf{E}_t &= \mathbf{p}_e \left[\cosh\left(\hat{\Gamma}\frac{\pm d}{2}\right)\mathbf{A} + \sinh\left(\hat{\Gamma}\frac{\pm d}{2}\right)\mathbf{B} \right] \\ &= \mathbf{p}_e \left[\check{\mathbf{A}} \pm \tanh\left(\hat{\Gamma}\frac{d}{2}\right)\check{\mathbf{B}} \right] \\ \mathbf{H}_t &= \mathbf{p}_h \left[\sinh\left(\hat{\Gamma}\frac{\pm d}{2}\right)\mathbf{A} + \cosh\left(\hat{\Gamma}\frac{\pm d}{2}\right)\mathbf{B} \right] \\ &= \mathbf{p}_e \left[\pm \tanh\left(\hat{\Gamma}\frac{d}{2}\right)\check{\mathbf{A}} + \check{\mathbf{B}} \right] \end{aligned} \tag{11}$$

with

$$\begin{aligned} \check{\mathbf{A}} &= \cosh\left(\hat{\Gamma}\frac{d}{2}\right)\mathbf{A} \\ \check{\mathbf{B}} &= \cosh\left(\hat{\Gamma}\frac{d}{2}\right)\mathbf{B} \end{aligned} \tag{12}$$

and

$$\mathbf{E}_t = \begin{bmatrix} \mathbf{E}_x \\ \mathbf{E}_y \end{bmatrix} = \boldsymbol{p}_e \hat{\Pi}; \quad \mathbf{H}_t = \begin{bmatrix} j\mathbf{H}_y \\ -j\mathbf{H}_x \end{bmatrix} = \boldsymbol{p}_h \hat{\mathbf{\Pi}}. \tag{13}$$

The different signs in (11) are valid for matching at the left and right boundary of the section. The difference operators $\boldsymbol{p}_e$ and $\boldsymbol{p}_h$ are described in Appendix B. A different number of lines in neighboring sections caused by a different distribution of the metallizations requires a partitioning of the matrices into two submatrices

$$\boldsymbol{p}_e = \begin{bmatrix} \boldsymbol{p}^r_e \\ \boldsymbol{p}^c_e \end{bmatrix}; \quad \boldsymbol{p}_h = \begin{bmatrix} \boldsymbol{p}^r_h \\ \boldsymbol{p}^c_h \end{bmatrix} \tag{14}$$

$\boldsymbol{p}^r_e$ and $\boldsymbol{p}^r_h$ correspond to the common discretization lines of the two sections. They have the same number of rows, whereas $\boldsymbol{p}^c_e$ and $\boldsymbol{p}^c_h$ denote the lines ending on the metallization of the other region. The matching procedure at the interface of two inner Sections I and II now yields

$$\begin{aligned} \mathbf{E}^I_t &= \mathbf{E}^{II}_t : \\ \boldsymbol{p}^{rI}_e(\hat{\mathbf{A}}^I - \gamma^I \tilde{\mathbf{B}}^I) &= \boldsymbol{p}^{rII}_e(\tilde{\mathbf{A}}^{II} + \gamma^{II}\tilde{\mathbf{B}}^{II}) \\ \boldsymbol{p}^{cI}_e(\tilde{\mathbf{A}}^I - \gamma^I \tilde{\mathbf{B}}^I) &= \mathbf{0} \\ \mathbf{0} &= \boldsymbol{p}^{cII}_e(\tilde{\mathbf{A}}^{II} + \gamma^{II}\tilde{\mathbf{B}}^{II}) \\ \mathbf{H}^I_t &= \mathbf{H}^{II}_t : \\ \boldsymbol{p}^{rI}_h(-\gamma^I \check{\mathbf{A}}^I + \check{\mathbf{B}}^I) &= \boldsymbol{p}^{rII}_h(\gamma^{II}\check{\mathbf{A}}^{II} + \check{\mathbf{B}}^{II}) \end{aligned} \tag{15}$$

with

$$\gamma^{I/II} = \tanh\left(\hat{\Gamma}^{I/II} \cdot \frac{d}{2}\right). \tag{16}$$

Now we combine the scattering matrices for the single discontinuities successively and obtain the generalized scattering matrix of the whole structure under study. For a given input—one or several of the propagating modes—the unknown amplitudes of the transmitted and reflected waves are computed.

III. Results

A. Investigation of Convergence

In order to determine the influence of the discretization, a simple stub filter (see Fig. 6) was analyzed as a test structure using three different numbers of discretization lines on the

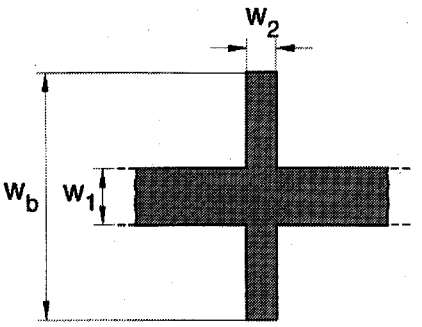

Fig. 6. Stub filter geometry $w_1 = 2.38$ mm, $w_2 = 2.38$ mm, $w_b = 20$ mm, $h_{sub} = 0.79$ mm, $\varepsilon_r = 2.35$.

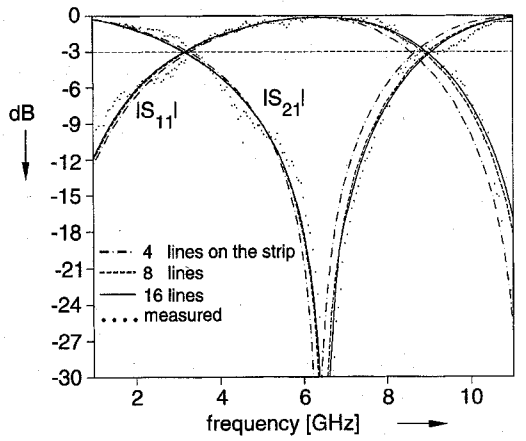

Fig. 7. Scattering parameters $|S_{11}|$ and $|S_{21}|$ for different line numbers of ϕ_x on the stripline w_1.

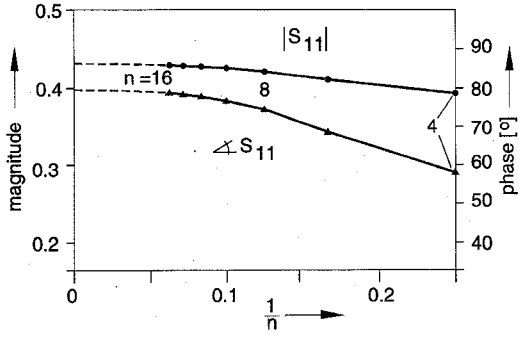

Fig. 8. Convergence of amplitude and phase of S_{11} for $f = 10$ GHz.

infinitely thin microstrip line. The scattering parameters are plotted in Fig. 7.

For an increasing number of lines the results shift toward the measured values [8]. In order to proof that a good accuracy has been achieved the convergence of amplitude and phase of the reflection coefficient is shown for the frequency $f = 10$ GHz. In Fig. 8 these values are plotted over the inverse number of lines n for the potential ϕ_x on the strip w_1. The result for $1/n \to 0$ is then obtained by an extrapolation.

To show the advantage of the reduction algorithm for a perfectly conducting metallization, the same analysis was performed by modeling the metallization as a dielectric medium with extremely high imaginary part of the dielectric constant. The results for the propagation constants and the scattering parameters are absolutely the same, but the required computation times differed extremely, which is shown in Fig. 8. The results are gained using MATLAB on a IBM RISC/6000 workstation. The explanation is the different treatment of real and complex tridiagonal matrices in the computation of the eigenvalues by the used LINPACK routines and the smaller size of the reduced matrices.

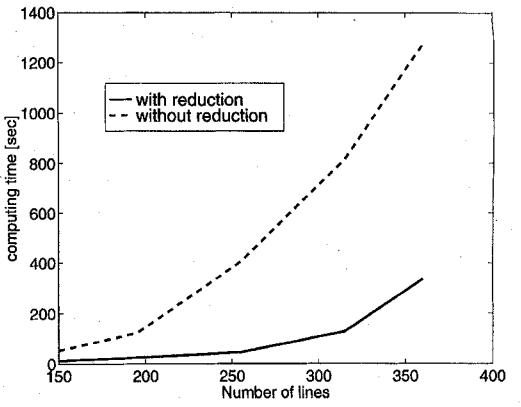

Fig. 9. Computing time for one frequency point versus number of ϕ_x lines in the cross section.

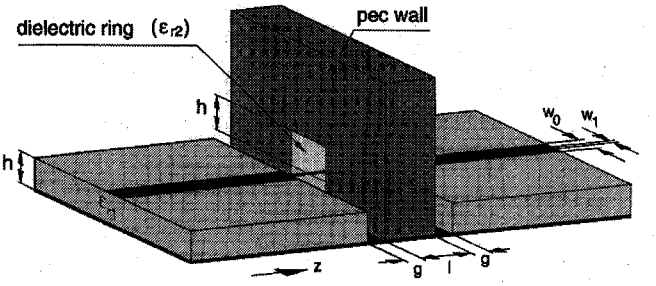

Fig. 10. Geometry of a hermetic bead transition [4] $w_0 = 0.55$ mm, $w_1 = 0.21$ mm, $\varepsilon_{r1} = \varepsilon_{r2} = 10.8$, $h = 0.635$ mm, $g = 0.4$ mm, and $l = 1.5$ mm.

B. Scattering Parameters for Various Structures

To demonstrate the versatility and accuracy of the new approach, which allows investigation of a great variety of 3-D structures using the same program, four different examples of transitions are investigated and compared with results published in literature.

The first example is a hermetic bead transition (Fig. 10), frequently encountered in encapsulated circuits to provide physical protection and electromagnetic shielding. The interconnecting coaxial line is approximated by a rectangular 50 Ω stripline as in [4]. The scattering parameters (Fig. 11) are in very good agreement with the other numerical methods [4].

The second example (Fig. 12) is a via hole, used for the connection of two 50-Ω striplines arranged in a three layer package [3]. The structure is divided into five regions, containing several metallizations of finite thickness. Fig. 13 is a plot of the S-parameters of the transition versus frequency. In contrast to [3] no artificial boundaries are necessary.

The third structure analyzed with the new algorithm is the connection of two microstrip lines by a bondwire (Fig. 14),

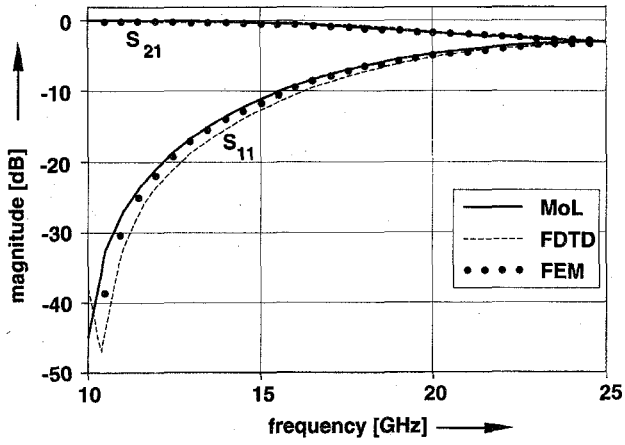

Fig. 11. Scattering parameters of a bead transition (Fig. 10) compared with FDTD [4] and FEM [4].

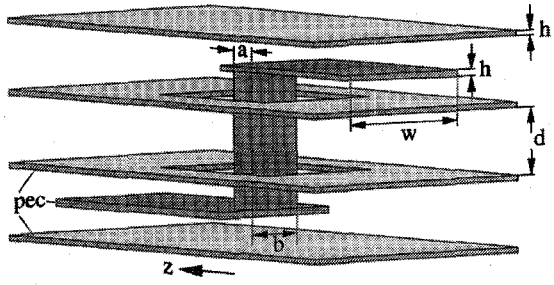

Fig. 12. Rectangular via connection of two striplines [3] $w = 1.25$ mm, $h = 0.25$ mm, $d = 1.25$ mm, $a = 0.5$ mm, and $b = 0.75$ mm.

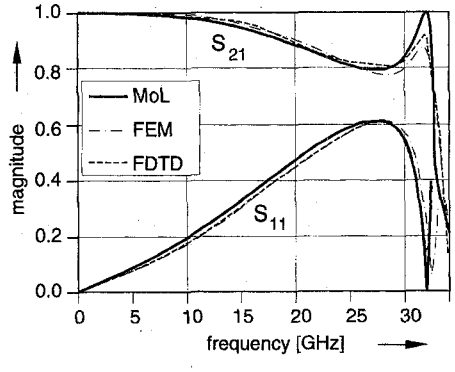

Fig. 13. S-parameters of the via connection (Fig. 12) in comparison with FEM and FDTD results in [3].

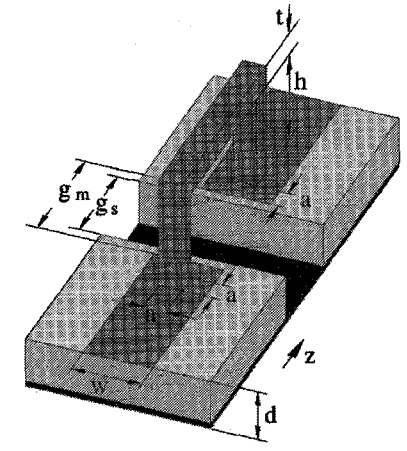

Fig. 14. Schematic view of an interconnection by a bondwire $w = 0.635$ mm, $a = 0.211$ mm, $\varepsilon_r = 9.8$, $d = 0.635$ mm, $h = 0.211$ mm, and $g_m = 0.635$ mm.

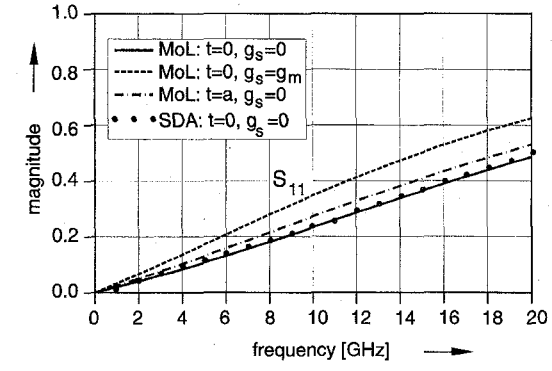

Fig. 15. Magnitude of the reflection coefficient for Fig. 14 in comparison to [6].

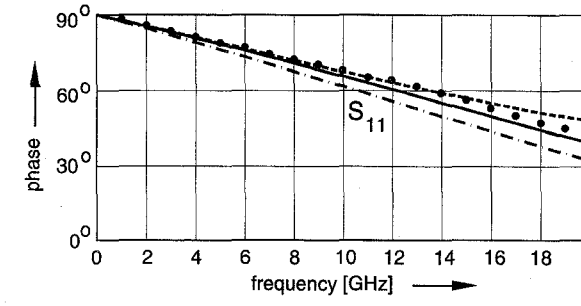

Fig. 16. Phase of the reflection coefficient (Fig. 14).

where the horizontal part of the wire is modeled as infinitely thin metallization [6]. Additionally, the influence of an air gap and the bondwire thickness on the circuit performance has been investigated. In Figs. 15 and 16 magnitude and phase of the computed reflection coefficient are sketched for different geometries in comparison to the results by the SDA [6], showing the influence of finite gap width and finite bondwire thickness. The horizontal bondwire thickness t and the air gap width g_s are used as parameters.

For the more realistic modeling of the bondwire with a metallization thickness $t = a$ a smaller magnitude of the reflection coefficient is visible.

The last example is a microstrip resonator filter on a lossy substrate, shown in Fig. 17. This structure is compared with an analysis by [2]. A similar structure on a lossless substrate was analyzed by [9], using also the method of lines, but with discretization lines perpendicular to the propagation direction. The dimension of the calculation window in the former MoL approach enforced the use of a vector computer, whereas with the new algorithm more accurate results were gained on a IBM RISC/6000 workstation using nearly half of the discretization lines.

For all four components our results are in good agreement with the results obtained by other methods. Even the phase, which is more sensitive against the influences of the discretization, is in good consistency with the results of [2] and [6].

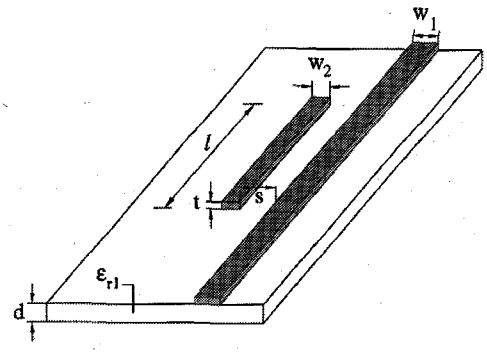

Fig. 17. Metallic parallel resonator exited by a microstrip line $w_1 = w_2 = 150\,\mu$m, $s = 75\,\mu$m, $\varepsilon_r = 12.9$, $\tan\delta = 10^{-2}$, $d = 150\,\mu$m, $t = 30\,\mu$m, and $l = 2.55$ mm.

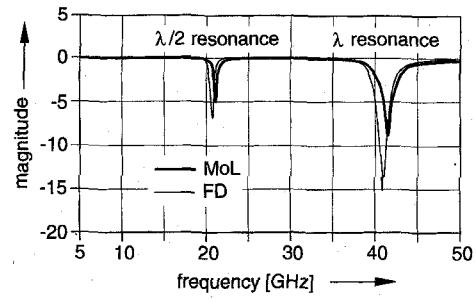

Fig. 18. Magnitude of the transmission coefficient of Fig. 16 in comparison to [2].

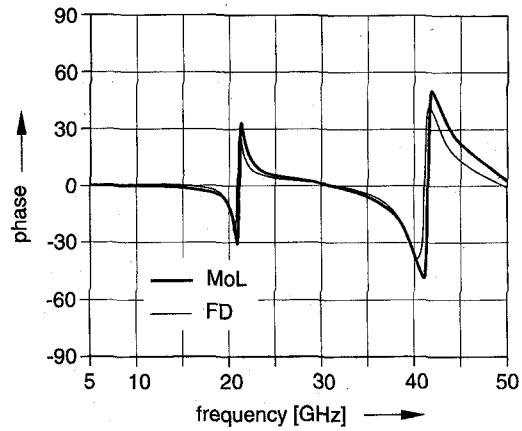

Fig. 19. Phase of the transmission coefficient.

IV. Conclusion

The main features of the proposed MoL approach can be summarized as follows: An advantage of this procedure is the analytical calculation in z direction. There is no need for special boundaries at the input and output. The size of the discretization window depends only on the cross section. This fact is extremely favorable for long structures or both long and short sections. High accuracy of the calculation is achieved by matching the field components instead of the modes. The use of different boundary conditions for the cross section makes the investigation of open and shielded structures possible. The scattering parameters are calculated directly, with an analytical distinction between the different modes. The easy mathematical description and the general formulation allow the analysis of a great variety of structures with the same program.

S-parameters for four different 3-D elements have been computed. A very good consistency with results published in literature can be stated both for magnitude and phase. The influence of air gaps and bondwire thickness was investigated, showing the suitability of the proposed approach for the analysis of 3-D interconnects.

Appendix A
Calculation of the Coupling Matrix

The components of the coupling matrix $\boldsymbol{Q}$ are described as following:

$$\hat{Q} = \begin{bmatrix} Q_{11} & Q_{12} \\ Q_{21} & Q_{22} \end{bmatrix} \tag{17}$$

with

$$\begin{aligned}
Q_{11} &= \frac{1}{\bar{h}_x^2}\hat{\varepsilon}^r_{\bullet}\hat{D}^{rt}_{xx}\hat{\varepsilon}^{r-1}_{\circ}\hat{D}^r_{xx} + \frac{1}{\bar{\bar{h}}_y^2}\hat{D}^{rt}_{xy}\hat{D}^r_{xy} - \hat{\varepsilon}^r_{\bullet} \\
Q_{12} &= \frac{1}{\bar{h}_x\bar{h}_y}\hat{\varepsilon}^r_{\bullet}\hat{D}^{rt}_{xx}\hat{\varepsilon}^{r-1}_{\circ}\hat{D}^r_{yy} - \frac{1}{\bar{\bar{h}}_x\bar{\bar{h}}_y}\hat{D}^{rt}_{xy}\hat{D}^r_{yx} \\
Q_{21} &= \frac{1}{\bar{\bar{h}}_x\bar{h}_y}\hat{\varepsilon}^r_{\blacktriangle}\hat{D}^{rt}_{yy}\hat{\varepsilon}^{r-1}_{\circ}\hat{D}^r_{xx} - \frac{1}{\bar{h}_x\bar{\bar{h}}_y}\hat{D}^{rt}_{yx}\hat{D}^r_{xx} \\
Q_{22} &= \frac{1}{\bar{h}_y^2}\hat{\varepsilon}^r_{\blacktriangle}\hat{D}^{rt}_{yy}\hat{\varepsilon}^{r-1}_{\circ}\hat{D}^r_{yy} + \frac{1}{\bar{\bar{h}}_x^2}\hat{D}^{rt}_{yx}\hat{D}^r_{yx} - \hat{\varepsilon}^r_{\blacktriangle}.
\end{aligned} \tag{18}$$

Appendix B
Calculation of the Field Components

The field components will be calculated from a potential $\boldsymbol{\Pi}$ by

$$\eta_0\mathbf{H} = j\nabla\times\boldsymbol{\Pi};\quad \mathbf{E} = \varepsilon_r^{-1}\nabla\times\nabla\times\boldsymbol{\Pi}. \tag{19}$$

In the discretized form we obtain the tangential fields by (13) with

$$\boldsymbol{p}_e = -\begin{bmatrix} \frac{1}{\bar{h}_x^2}\hat{D}^{rt}_{xx}\hat{\varepsilon}^{r-1}_{\circ}\hat{D}^r_{xx} - \hat{I}_{N\circ} & \frac{1}{\bar{h}_x\bar{h}_y}\hat{D}^{rt}_{xx}\hat{\varepsilon}^{r-1}_{\circ}\hat{D}^r_{yy} \\ \frac{1}{\bar{h}_x\bar{h}_y}\hat{D}^{rt}_{yy}\cdot\hat{\varepsilon}^{r-1}_{\triangle}\hat{D}^r_{xx} & \frac{1}{\bar{h}_y^2}\hat{D}^{rt}_{yy}\hat{\varepsilon}^{r-1}_{\triangle}\hat{D}^r_{yy} - \hat{I}_{N\blacktriangle} \end{bmatrix} \tag{20}$$

and

$$\boldsymbol{p}_h = -\hat{\boldsymbol{T}}\hat{\boldsymbol{\Gamma}}. \tag{21}$$

The matrices $\hat{\boldsymbol{I}}_N$ are identity matrices of the size of the corresponding reduced line system. For the description of the fields the self-adjoint formulation is chosen.

References

[1] A. Christ and H. L. Hartnagel, "Three-dimensional finite-difference method for the analysis of microwave-device embedding," *IEEE Trans. Microwave Theory Tech.*, vol. 35, pp. 688–696, 1987.

[2] D. Hollmann, "Field theoretical methods for the analysis of dielectric resonators in integrated microwave devices," (in German), Ph.D. dissertation, Karlsruhe, 1991.

[3] J. Wang and R. Mittra, "Finite element analysis of MMIC structures and electronic packages using absorbing boundary conditions," *IEEE Trans. Microwave Theory Tech.*, vol. 42, no. 3, pp. 441–449, 1994.
[4] J. Yook, N. I. Dib, E. Yasan, and L. P. B. Katehi, "A study of hermetic transitions for microwave packages," in *Microwave Theory Techniques Symp., IEEE MTT-S Dig.*, Orlando, May 1995, pp. 1579–1582.
[5] H. Jin, R. Vahldieck, and J. Huang, "Rigorous analysis of mixed transmission line interconnects using the frequency-domain TLM method," *IEEE Trans. Microwave Theory Tech.*, vol. 41, no. 12, pp. 2248–2255, 1993.
[6] T. Becks and I. Wolff, "Analysis of 3-D metallization structures by a full-wave spectral domain techniques," *IEEE Trans. Microwave Theory Tech.*, vol. 40, no. 12, pp. 2219–2227, 1992.
[7] R. Pregla and W. Pascher, "The method of lines," in *Numerical Techniques for Microwave and Millimeter Wave Passive Structures,* T. Itoh, Ed. New York: Wiley, 1989, pp. 381–446.
[8] S. B. Worm, "Full-wave analysis of discontinuities in planar waveguides by the method of lines using a source approach," *IEEE Trans. Microwave Theory Tech.*, vol. 38, pp. 1510–1514, 1990.
[9] A. Kornatz and R. Pregla, "Full wave analysis of microstrip filters containing dielectric and metallic resonators with the method of lines," in *Microwave Theory Techniques Symp., IEEE MTT-S Dig.*, Orlando, May 1995, pp. 649–652.
[10] R. Pregla, "MoL–BPM method of lines based beam propagation method," in *Methods for Modeling and Simulation of Guided-Wave Optoelectronic Dev.*, W. P. Huang, Ed. Cambridge, MA: EMW Publishing, 1995, no. PIER 11 in Progress in Electromagnetic Research, pp. 51–102.
[11] W. Pascher and R. Pregla, "Analysis of rectangular waveguide discontinuities by the method of lines," *IEEE Trans. Microwave Theory Tech.*, vol. 43, no. 2, pp. 416–420, Feb. 1995.
[12] L. Vietzorreck and R. Pregla, "Analysis of Discontinuities in microwave circuits with a new eigenmode algorithm based on the method of lines," in *25th Eur. Microwave Conf.*, Bologna, Italy, Sept. 1995, pp. 804–808.

Larissa Vietzorreck (M'96) was born in Düsseldorf, Germany, in 1965. She received the master's degree in electrical engineering (Dipl. Ing.) from the Ruhr Universität Bochum, Germany, in 1992.

Since 1992, she has been a Research Assistant in the Department of Electrical Engineering of the FernUniversität, Hagen, Germany, where she is working toward her doctoral degree. Her research interests are numerical modeling of planar microwave components and printed antennas.

Reinhold Pregla (M'76–SM'83) received the master's degree in electrical engineering (Dipl. Ing.) and the doctorate engineering (Dr. Ing.) from the Technical University Braunschweig, West Germany, in 1963 and 1966, respectively.

From 1966 to 1969, he was a Research Assistant in the Department of Electrical Engineering of the Technical University Braunschweig (Institut für Hochfrequenztechnik), where he was engaged in investigations of microwave filters. After the Habilitation, he was a Lecturer in high frequencies at the Technical University Braunschweig. Since 1973, he has held the position of Professor at the Ruhr—University Bochum, Germany, and since 1975, he has been a full Professor in Electrical Engineering at the FernUniversität (a university for distance study) in Hagen, Germany. His fields of investigation include microwave passive circuits, waveguide theory for microwaves and optics, antennas, and laser modeling.